Effects of rare-earth ion size on the stability of the coherent Jahn-Teller distortions in undoped perovskite manganites

T. F. Seman and K. H. Ahn*
Department of Physics, New Jersey Institute of Technology, Newark, New Jersey 07102, USA

T. Lookman, A. Saxena, and A. R. Bishop
Theoretical Division, Los Alamos National Laboratory, Los Alamos, New Mexico 87545, USA

P. B. Littlewood
Physical Sciences and Engineering Division, Argonne National Laboratory, Argonne, Illinois 60439, USA
(Received 9 August 2012; published 12 November 2012)

We present a theoretical study on the relation between the size of the rare earth ion, often known as chemical pressure, and the stability of the coherent Jahn-Teller distortions in undoped perovskite manganites. Using a Keating model expressed in terms of atomic scale symmetry modes for a simplified two-dimensional model, we show that there exists a coupling between the uniform shear distortion and the staggered buckling distortion within the Jahn-Teller energy term. It is found that this coupling provides a mechanism by which the coherent Jahn-Teller distortion is more stabilized by a smaller rare earth ion. We analyze the appearance of the uniform shear distortion below the Jahn-Teller ordering temperature, estimate the Jahn-Teller ordering temperature and its variation among $LaMnO_3$, $PrMnO_3$, and $NdMnO_3$, and obtain the relations between distortions. We find good agreement between theoretical results and experimental data.

DOI: 10.1103/PhysRevB.86.184106 PACS number(s): 75.47.Gk, 74.62.Dh, 64.70.K−, 61.50.Ks

I. INTRODUCTION

Since the discovery of the colossal magnetoresistance effect, a lot of attention has focused on a class of materials known as perovskite manganites.[1–3] During the last two decades, substantial progress has been made in the theory for perovskite manganites. Importance of the electron-lattice coupling was identified shortly after the discovery of colossal magnetoresistance effect.[4–6] First-order character of the metal-insulator phase transition has been found from Monte Carlo simulations.[7] Mechanism for inhomogeneity and its relation to metal-insulator transition have been studied.[8] Effects of disorder have been investigated for doped manganites.[9,10] The competition between short range super-exchange interaction and long range double exchange interaction has been analyzed for multiferroic undoped manganites.[11] Most recently, novel mechanisms for ferroelectricity, including electronic ferroelectricity, have been proposed for undoped manganites with E-type antiferromagnetic ordering.[12,13] These materials have the chemical formula in the form of $RE_{1-x}AK_xMnO_3$, where RE and AK represent the rare earth and alkali metal elements, and have a perovskite structure. One of the major research themes for these materials is the relation between their physical properties and the average size of ions at the RE/AK site, often known as the chemical pressure effect. The size of the RE/AK ion is usually parameterized by a *tolerance factor*, and one of the most important phase diagrams for these materials has been the one in the temperature versus tolerance factor plane for a fixed 30% ($x = 0.3$) doping ratio.[14] The RE/AK ions with size smaller than the space created by the surrounding MnO_6 octahedra induce buckling of the Mn-O-Mn bonds, observed through various structural refinement analyses.

To understand the effect of the chemical pressure, semiclassical theories[4–13] with quantum mechanical electrons coupled with the classical lattice through the Jahn-Teller (JT) interaction often present the phase diagram with one axis representing the ratio between the electron hopping energy and the JT energy gain. This ratio parameterizes the competition between the kinetic and potential energy in perovskite manganites. Theoretical phase diagrams from these approaches agree well with experimental phase diagrams, when this ratio is related to the Mn-O-Mn buckling distortion due to smaller RE/AK ions. However, whether this buckling distortion affects the electron hopping energy or the JT energy gain has been controversial. It is well known from experimental observations that there is a strong competition between the insulating phase with a coherent JT distortion and the metallic phase without such distortion.[3] So far, most of the attention has centered on the impact of the buckling on the metallic phase, in particular, the possible change in the effective Mn-O-Mn electron hopping parameter and the band width.[14] At the same time, there has been a debate whether the variation of the hopping parameter due to the Mn-O-Mn bond angle change of several degrees would be significant enough to explain the observed metal-insulator transition.[15–19] For instance, the spin wave stiffness, which depends sensitively on the electron hopping amplitude in double exchange model in ferromagnetic metallic phase, shows very little dependence on Mn-O-Mn bond angle.[16,18] A less studied effect of the Mn-O-Mn bond buckling, except for a few early efforts based on experimental data,[20] is the possibility that the buckling distortion may significantly stabilize the insulating phase with a coherent JT distortion, by affecting the JT energy gain. The main goal of this paper is to examine such a possibility with a simplified model of the perovskite manganites. To be specific, we analyze the interplay between the JT ordering and chemical pressure for undoped perovskite manganites. With one localized e_g electron per site, the electronic degrees

of freedom can be integrated out in undoped manganites (except for electronically ferroelectric undoped manganites postulated at low temperatures for very small RE ions), which allows us to adopt a purely classical model with the energy expressed in terms of lattice distortions only. The study on undoped manganites is merited, because they are not only parent compounds of doped perovskite manganites,[21] but also because one of the first multiferroic materials discovered is an undoped manganite, $TbMnO_3$, with a relatively small RE element.[22] Recently, electronic ferroelectricity has been also proposed for undoped perovskite manganites.[12,13] Therefore, the chemical pressure effect in undoped manganites reported in this paper would also be relevant for future studies on how the multiferroic and electronically ferroelectric properties would appear in $REMnO_3$ with small RE ions, as well as how the chemical pressure affects the distorted insulating phase of doped manganites.

II. MODEL SYSTEM AND ENERGY EXPRESSION

We study a two-dimensional (2D) model for the perovskite structure which incorporates both buckling and the JT distortions. We define a 2D perovskite structure shown in Fig. 1 which includes the following aspects of the three-dimensional (3D) perovskite structure for undoped manganites: (1) symmetry breaking distortion of O ions around Mn ion, (2) chemical pressure effect, which is the attraction of surrounding O ions toward the small RE ions, and (3) the rotation of O ions with alternating directions around Mn ions, which is, in effect, the buckling of Mn-O-Mn bonds. Although our 2D model inevitably misses some aspects of 3D lattice distortions, we propose that we can still achieve the correct order of magnitude estimation of energies associated with the chemical pressure and the JT effect. For example, the size of the 3D tetragonal JT distortion mode, commonly known as Q_3 mode[23] with Mn-O bond lengths changed in all directions, is typically about a third of the size of the planar JT distortion mode, commonly known as Q_2 mode with Mn-O bond lengths changed only in the plane. The Q_2 mode is kept in our 2D model, but the Q_3 mode is not. The error from omitting the Q_3 mode in our 2D model can be estimated by comparing actual 3D and our approximate 2D Jahn-Teller energy gain, proportional to $\sqrt{Q_2^2+Q_3^2}$ and $\sqrt{Q_2^2}$, respectively, which are different by only about 10%. The Q_2 mode is expected to couple dominantly

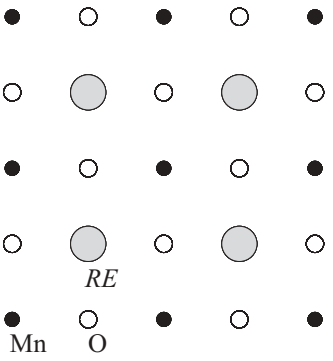

FIG. 1. Two-dimensional model for the perovskite structure considered in the text.

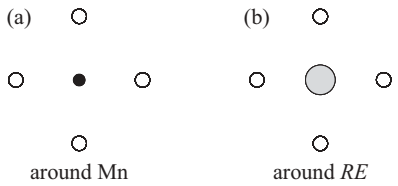

FIG. 2. Two structural motifs chosen for the 2D structure shown in Fig. 1.

with the in-plane Mn-O-Mn bond buckling and the in-plane contraction of O ions surrounding a small RE ion. Therefore, we expect that our 2D model would be sufficient for an order of magnitude estimation of the energy associated with the stabilization of the phase with the JT distortion by small RE ions.

For our 2D model of perovskite structure, we apply the recently developed atomic scale description of lattice distortions[24,25] to describe the elastic energy of the system. In this approach, atomic scale modes of lattice distortions and their constraints are used instead of displacement variables. The structural motifs can be chosen in any convenient way as long as they have the symmetry of the crystal structure. We choose two "structural motifs" shown in Fig. 2: One consists of one Mn ion and four surrounding O ions and the other comprises one RE ion and four surrounding O ions. We obtain ten symmetry modes for each motif, shown in Fig. 3 for the MnO_4 motif.[26] Similar symmetry modes are defined for the REO_4 motif and are distinguished with primes on the symbols in this paper. The modes defined for each plaquette on the lattice are constrained by each other because neighboring motifs share ions, which leads to constraint equations between

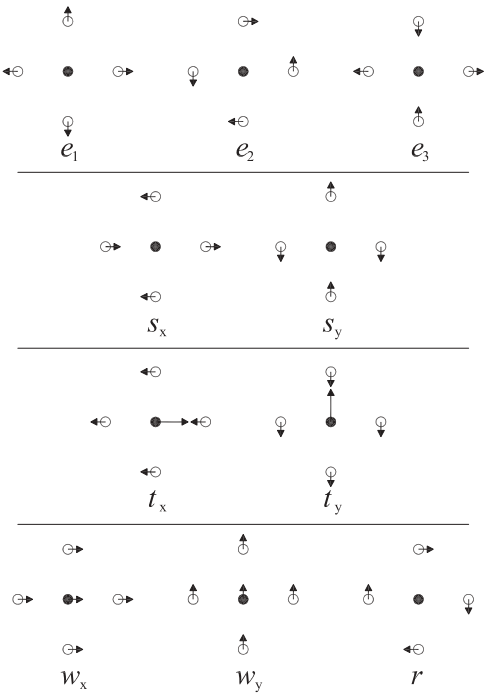

FIG. 3. Distortion modes for the motif around the Mn ion in Fig. 2. Similar distortion modes e_1', e_2', e_3', s_x', s_y', t_x', t_y', w_x', w_y', and r' are defined for the motif around the RE ion.

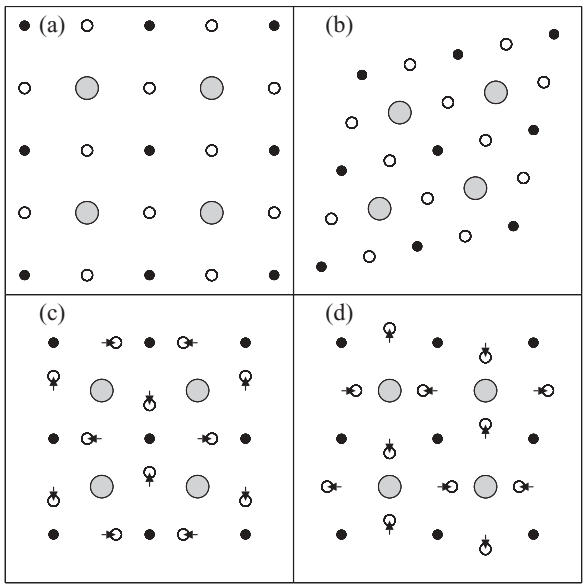

FIG. 4. Four distortion modes considered in the current study: (a) uniform dilatation mode e_{10}, (b) uniform shear mode e_{20}, (c) staggered deviatoric mode e_{3s}, and (d) staggered buckling mode e'_{3s}. All figures are drawn for the positive values of the modes with the Mn site at the bottom left corner chosen as the origin.

the Fourier components of the modes. In terms of these twenty modes and constraint equations, any distortion of the 2D perovskite structure shown in Fig. 1 can be described.

For the current study, since we are interested in the ordered state, we consider distortions with wave vectors $\vec{k} = (0,0)$ and (π,π) only. For these wave vectors, the constraint equations are as follows, where we use subscripts 0 and s to represent $\vec{k} = (0,0)$ and (π,π), respectively: $e_{10} = e'_{10}$, $e_{20} = e'_{20}$, $e_{30} = e'_{30}$, $s_{x0} = -s'_{x0}$, $s_{y0} = -s'_{y0}$, $e_{1s} = -e'_{2s}$, $e'_{1s} = -e_{2s}$, $s_{xs} = s_{ys} = s'_{xs} = s'_{ys} = 0$. The rest of the modes are unconstrained, particularly e_{3s} and e'_{3s}. We search for the interplay between the staggered deviatoric distortion mode e_{3s} and the staggered rotation of O ions around Mn ion (or equivalently staggered Mn-O-Mn bond buckling mode) e'_{3s}, where the latter is due to the compression $e'_{10} = e_{10}$ by small RE ions. Therefore, we limit ourselves to the modes $e_{10} = e'_{10}$, $e_{20} = e'_{20}$, e_{3s}, and e'_{3s}, shown in Fig. 4. We include the uniform shear mode $e_{20} = e'_{20}$ because it is coupled to e'_{3s} through the JT term, as will be discussed later in this paper.

Even though it is possible to analyze an energy expression including higher order symmetry-allowed anharmonic energy terms, such a method would generate many parameters and would make the model less predictive. Therefore, we start with a Keating model with a small number of parameters[27,28] and map the Keating model onto the approach based on the symmetry modes. In the Keating approach, the elastic energy is represented in terms of bond length and bond angle changes from equilibrium. For our 2D perovskite structure, we consider the following set of Keating variables and harmonic moduli for each Mn ion, as shown in Fig. 5: δl_n $(n = 1, 2, 3, 4)$ and modulus a_1 for Mn-O bond length change, $\delta\theta_n$ $(n = 1, 2, 3, 4)$ and $b_1/4$ for 90° O-Mn-O bond angle change, δr_n $(n = 1, 2, 3, 4)$ and a_2 for RE-O bond length change, and $\delta\varphi_n$ $(n = 1, 2)$ and $b_2/4$ for 180° Mn-O-Mn bond angle change. We note that the

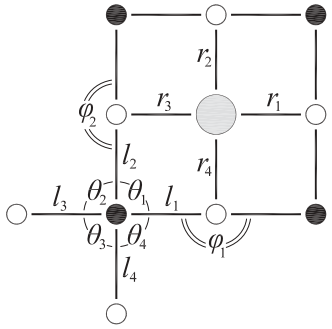

FIG. 5. The Keating variables considered for each Mn ion. l_1, l_2, l_3, and l_4 represent the Mn-O bond lengths. θ_1, θ_2, θ_3, and θ_4 represent the O-Mn-O bond angles. r_1, r_2, r_3, and r_4 represent RE-O bond lengths. φ_1 and φ_2 indicate Mn-O-Mn bond angles.

MnO_4 motif is considered as relatively stiff compared to other components of the structure, so that $a_1 \gg a_2$ and $b_1 \gg b_2$.

We consider the following Keating elastic energy expression per Mn ion,

$$E_{\text{elastic}} = \frac{1}{2}a_1 \sum_{n=1,2,3,4} (\delta l_n)^2 + \frac{1}{2}b_1 \sum_{n=1,2,3,4} (\delta\theta_n/2)^2 + \frac{1}{2}a_2 \sum_{n=1,2,3,4} (\delta r_n)^2 + \frac{1}{2}b_2 \sum_{n=1,2} (\delta\varphi_n/2)^2. \quad (1)$$

We express the Keating variables in terms of e_{10}, e_{20}, e_{3s}, and e'_{3s}. For example, we obtain

$$\delta l_1 = \frac{\sqrt{(1 + e_{10} + e_{3s})^2 + (e_{20} + e'_{3s})^2} - 1}{2}, \quad (2)$$

$$\delta\theta_1 = \tan^{-1}\left(\frac{e_{20} + e'_{3s}}{1 + e_{10} + e_{3s}}\right) + \tan^{-1}\left(\frac{e_{20} - e'_{3s}}{1 + e_{10} - e_{3s}}\right). \quad (3)$$

The Taylor expansion of E_{elastic} in terms of e_{10}, e_{20}, e_{3s}, and e'_{3s} produces all the terms of any order. We make an approximation that b_2 is much smaller than other parameters, as mentioned above, and drop the terms with b_2. We keep all harmonic order terms and select the cubic and quartic order terms that are responsible for the Mn-O-Mn bond buckling instability, which are shown below as E_{har}, E_{cubic}, and E_{quartic}.

We further define the JT energy per Mn ion E_{JT} and the energy associated with the tolerance factor per Mn ion E_{tol} as follows:

$$E_{\text{JT}} = -\frac{\lambda}{2}|\delta l_1 + \delta l_3 - \delta l_2 - \delta l_4|, \quad (4)$$

$$E_{\text{tol}} = \frac{\tilde{p}}{2}(\delta r_1 + \delta r_2 + \delta r_3 + \delta r_4), \quad (5)$$

where we define "chemical pressure" as

$$\tilde{p} = C'_1(1 - t). \quad (6)$$

The parameter t is a two-dimensional analog of the tolerance factor for the 3D perovskite structure, and the coefficient C'_1 represents the coupling between the average RE-O bond length and the tolerance factor t. The chemical pressure $\tilde{p}$ induces the shortening of the average RE-O bond length due to small RE ions. We also define the JT distortion mode

$$e_{\text{JT}} = (\delta l_1 + \delta l_3 - \delta l_2 - \delta l_4)/2, \quad (7)$$

which represents the anisotropic bond length change, similar to the JT distortion modes Q_2 and Q_3 for 3D perovskite manganites.[23] As mentioned above, $e_{\rm JT}$ in our 2D model corresponds to Q_2 mode only and we omit Q_3 mode. The expression $E_{\rm JT} = -\lambda|e_{\rm JT}|$ is based on the 3D JT energy $E_{\rm JT,3D} = -\lambda_Q\sqrt{Q_2^2+Q_3^2}$, which is obtained after minimizing JT electron-lattice coupling energy in manganites with respect to the e_g orbital state.[23] In undoped manganites, Q_3/Q_2 is about 0.3–0.4 (Refs. 29 and 30), which allows an approximation $E_{\rm JT,3D} \approx -\lambda_Q|Q_2|[1+(Q_3/Q_2)^2/2]$. Further neglecting the small $(Q_3/Q_2)^2/2$ term of about 0.1, we get the 2D analog of the JT energy $E_{\rm JT}$ with the 2D JT distortion $e_{\rm JT}$ corresponding to 3D JT distortion Q_2 except for a normalization factor difference.

We expand $E_{\rm JT}$ and $E_{\rm tol}$ in the form of a Taylor series in e_{10}, e_{20}, e_{3s}, and e'_{3s}. Only the leading order energy terms being kept, our total energy expression per Mn ion $E_{\rm tot}$ is given below.

$$E_{\rm tot} = E_{\rm har} + E_{\rm JT} + E_{\rm tol} + E_{\rm cubic} + E_{\rm quartic}, \tag{8}$$

$$E_{\rm har} = \tfrac{1}{2}(a_1+a_2)(e_{10})^2 + \tfrac{1}{2}(4b_1)(e_{20})^2 + \tfrac{1}{2}a_1e_{3s}^2 + \tfrac{1}{2}a_2(e'_{3s})^2, \tag{9}$$

$$E_{\rm JT} = -\lambda|e_{3s} + e_{20}e'_{3s}|, \tag{10}$$

$$E_{\rm tol} = \tilde{p}e_{10}, \tag{11}$$

$$E_{\rm cubic} = \tfrac{1}{2}a_1e_{10}(e'_{3s})^2, \tag{12}$$

$$E_{\rm quartic} = \tfrac{1}{4}\frac{a_1}{2}(e'_{3s})^4, \tag{13}$$

where the relation

$$e_{\rm JT} \approx e_{3s} + e_{20}e'_{3s} \tag{14}$$

is used for $E_{\rm JT}$. The physical origin of the coupling between e_{20} and e'_{3s} is important for the current study and is explained in more detail in Sec. V A.

III. ESTIMATION OF PARAMETERS

In this section, we present our estimate of the parameters. We choose the Mn-Mn distance before the distortion, which is around $u = 4$ Å, as 1. Therefore, e_{10}, e_{20}, e_{3s}, and e'_{3s} are unitless, and a_1, b_1, a_2, b_2, and λ have the unit of energy. The parameter a_1 can be estimated from the Mn-O bond stretching phonon mode energy, which is about 70 meV from optical measurements.[23] From $\hbar\sqrt{2a_1/m_{\rm O}} = 70$ meV with $m_{\rm O}$ the mass of the O ion, we obtain $a_1 \approx 150$ eV. We estimate b_1 from the elastic modulus, c_{44}. From Ref. 31, $c_{44} \approx$ 55–60 GPa. The uniform shear mode e_{20} corresponds to the conventional $e_{xy}/2$ (Ref. 32). Using the identity 1 GPa Å^3 = 6.3 meV, we find $b_1 \approx$ 20–25 eV. To estimate b_2, we use the results[33] for ReO_3, which has no RE/AK ion and, therefore, $a_2 = 0$ and the buckling of Re-O-Re bond depends only on b_2. According to the analysis in Ref. 33, the oxygen oscillation along Re-O-Re direction has the angular frequency $\omega_o^x = 905$ cm^{-1}, whereas the oscillation perpendicular to Re-O-Re direction has the angular frequency $\omega_o^y = 30$ cm^{-1}, from which we can estimate $b_2/a_1 = (\omega_o^y/\omega_o^x)^2/2 \approx 0.5\times10^{-3}$. We can expect a similar order of magnitude for b_2 in manganites, order of $10^{-3}a_1$, for example 0.2 eV, which is negligible compared to other parameter values and justifies neglecting the terms with b_2 as mentioned above. Various probes, such as neutron or optical spectroscopy, indicate the buckling mode frequency in manganites of about 35–50 meV (Ref. 34). From the analysis of (π,π) phonon mode for our model, we obtain the frequency of buckling mode $\omega_{\rm bk} = \sqrt{(2a_2+4b_2)/m_{\rm O}}$. Therefore, we obtain $a_2 \approx$ 30–80 eV. For the estimation of λ, we match the JT energy gain for our 2D model with that for the 3D model to ensure that our 2D model represents the energy scale of the 3D materials correctly. For our 2D model $\Delta E_{\rm JT} = -\lambda^2/(2a_1)$. For the 3D model in Refs. 23 and 35, $\Delta E_{\rm JT} \approx -0.39$ eV, and therefore, we obtain $\lambda \approx 10.8$ eV.

IV. INTERPLAY BETWEEN Mn-O-Mn BOND BUCKLING AND THE JAHN-TELLER DISTORTIONS

A. Buckling instability without the Jahn-Teller term

We find the condition for the buckling instability without the effect of the JT energy term $E_{\rm JT}$. We take a perturbative approach rather than try to solve high order polynomial equations. By minimizing $E_{\rm har} + E_{\rm tol}$, we obtain

$$(e_{10})^{\min,*} = -\frac{\tilde{p}}{a_1+a_2}, \tag{15}$$

where the superscript * indicates that the JT term is not yet taken into consideration. This isotropic compression of the MnO_4 motif renormalizes the coefficient of the $(e'_{3s})^2$ term through the $E_{\rm cubic}$ term. From this, we obtain the critical condition for the buckling instability,

$$\tilde{p}_c^* = \frac{a_2}{a_1}(a_1+a_2), \tag{16}$$

$$(e_{10})_c^{\min,*} = -\frac{a_2}{a_1}. \tag{17}$$

If $\tilde{p} > \tilde{p}_c^*$, Mn-O-Mn bond buckling occurs and the quartic order term $E_{\rm quartic}$ should be considered for the equilibrium e'_{3s},

$$|(e'_{3s})^{\min,*}| = \sqrt{\frac{2}{a_1+a_2}}\sqrt{\tilde{p}-\tilde{p}_c^*} \tag{18}$$

$$= \sqrt{2}\sqrt{(e_{10})_c^{\min,*} - (e_{10})^{\min,*}}. \tag{19}$$

The minimized $E_{\rm tot}$ without the $E_{\rm JT}$ term is given by

$$E_{\rm tot}^{\min,*} = -\frac{\tilde{p}^2}{2(a_1+a_2)} - \frac{a_1}{2}\left(\frac{\tilde{p}}{a_1+a_2} - \frac{a_2}{a_1}\right)^2. \tag{20}$$

B. Buckling instability with the Jahn-Teller term

We now examine how the JT energy term $E_{\rm JT}$ alters the buckling instability. From $E_{\rm har} + E_{\rm tol} + E_{\rm JT}$, we

obtain

$$(e_{10})^{\min} = -\frac{\tilde{p}}{a_1 + a_2}, \tag{21}$$

$$(e_{3s})^{\min} = \frac{\lambda}{a_1}, \tag{22}$$

where we consider the $(e_{3s})^{\min} > 0$ case only. The buckling instability is found from the second order terms in e_{20} and e'_{3s} in $E_{\rm tot}$:

$$\tfrac{1}{2}(4b_1)(e_{20})^2 + \tfrac{1}{2}[a_2 + a_1(e_{10})^{\min}](e'_{3s})^2 - \lambda e_{20} e'_{3s}, \tag{23}$$

where we assumed $(e_{3s})^{\min} + e_{20}e'_{3s} > 0$. From the condition $4b_1[a_2 + a_1(e_{10})^{\min}] < \lambda^2$, we obtain the critical condition

$$\tilde{p}_c = \frac{a_2}{a_1}(a_1 + a_2) - \frac{\lambda^2}{4b_1 a_1}(a_1 + a_2), \tag{24}$$

and the buckling distortion occurs for $\tilde{p} > \tilde{p}_c$. Comparing with $\tilde{p}^*_c$ in Eq. (16), we find that the JT energy makes buckling more likely. After this buckling instability, we should include the $E_{\rm quartic}$ term to find the equilibrium result. For this, we first minimize $E_{\rm tot}$ with respect to the shear distortion e_{20} to obtain

$$(e_{20})^{\min} = \frac{\lambda}{4b_1} e'_{3s}. \tag{25}$$

Inserting this back, we get an energy expression for $E_{\rm tot}$ in terms of e'_{3s} only, which gives the equilibrium buckling distortion and the minimum energy,

$$(e'_{3s})^{\min} = \sqrt{\frac{2}{a_1 + a_2}}\sqrt{\tilde{p} - \tilde{p}_c}, \tag{26}$$

$$E_{\rm tot}^{\min} = -\frac{\tilde{p}^2}{2(a_1 + a_2)} - \frac{\lambda^2}{2a_1} - \frac{a_1}{2}\left(\frac{\tilde{p}}{a_1 + a_2} - \frac{a_2}{a_1} + \frac{\lambda^2}{4b_1 a_1}\right)^2. \tag{27}$$

Therefore, the energy gain due to the JT energy term is given by

$$\Delta E_{\rm JT} = -\frac{\lambda^2}{2a_1} - \frac{(\tilde{p} - \tilde{p}^*_c)\lambda^2}{4(a_1 + a_2)b_1} \tag{28}$$

up to order λ^2. The second term corresponds to the part of $\Delta E_{\rm JT}$ which depends on the size of RE ion, or $\tilde{p}$. This result shows that the small rare earth ion, or large chemical pressure, stabilizes the JT distortion.

V. COMPARISON WITH EXPERIMENTS

We make comparisons between our model and experimental results. In Sec. V A, we explain the simultaneous appearance of the uniform shear distortion and the long range JT distortion observed in undoped manganites.[29] In Sec. V B, we estimate the changes in the JT ordering temperature $T_{\rm JT}$ among $LaMnO_3$, $PrMnO_3$, and $NdMnO_3$, and compare with experiments. In Sec. V C, we calculate the ratios between different distortion modes and compare with experimental data for $LaMnO_3$, $PrMnO_3$, $NdMnO_3$, and other undoped manganites with even smaller RE ions.

A. Appearance of uniform shear distortion below the Jahn-Teller ordering temperature

Experimental data in Refs. 29, 30, and 36 show that the difference between the lattice constants a and b along the diagonal directions in the plane appears simultaneously with the long range JT distortion below $T_{\rm JT}$ for $LaMnO_3$, $PrMnO_3$, and $NdMnO_3$. This distortion corresponds to the uniform shear distortion in our model, related by $e_{20} = (b - a)/(2\sqrt{2}u)$ with $u = 4$ Å. We analyze the coupling between the JT distortion and the uniform shear distortion, which is important for the stabilization of JT ordered state by the chemical pressure. In our model, such coupling originates from the term $e_{20}e'_{3s}$ in $e_{\rm JT}$ in Eq. (14) or in $E_{\rm JT}$ in Eq. (10), which can be understood as follows. We consider applying a positive e_{20} shear distortion to the lattice, as shown in Fig. 6 by the axis of elongation and compression along 45° and 135°, respectively. Such uniform shear distortion makes the Mn-O bond lengths either longer or shorter depending on whether the direction of the bond is closer to the orientation of elongation (45°) or compression (135°), except for the bonds with directions right between the two directions. If the system *does not* have (π,π) buckling, as shown by the *thin* solid lines in Fig. 6, all Mn-O bonds make equal angles from the axis of elongation/compression, and therefore e_{20} shear distortion keeps all Mn-O bond lengths equal. This implies that e_{20} distortion alone does not contribute to the JT distortion or JT energy gain. In contrast, if the system has a buckling distortion e'_{3s} with a wave vector $\vec{k} = (\pi,\pi)$, as shown by the *thick* solid lines in Fig. 6, the e_{20} shear distortion elongates Mn-O bonds marked with l and shortens Mn-O bonds marked with s, depending on whether the bond direction is closer to the axis of elongation or the axis of compression, which results in the JT distortion $e_{\rm JT}$ with a

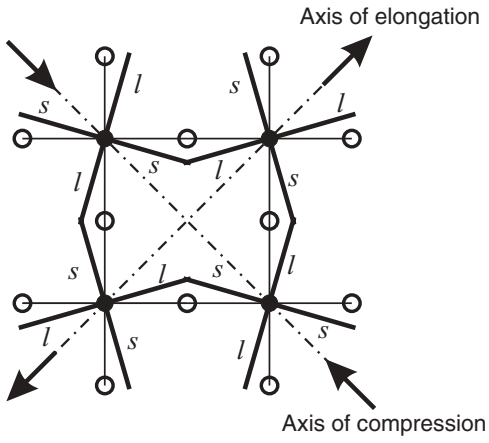

FIG. 6. Superposition of (π,π) buckling e'_{3s} and uniform shear distortion e_{20} effectively generates the extra (π,π) JT distortion of Mn-O bond lengths, as indicated by the s and l for the shortened and elongated bonds, which is responsible for the $e_{20}e'_{3s}$ coupling within $e_{\rm JT}$ and the JT coupling $E_{\rm JT}$. In the (π,π) JT ordered state, this adds up to the e_{3s} deviatoric mode if e_{3s} and $e_{20}e'_{3s}$ have the same sign. This mechanism is responsible for the appearance of the uniform shear distortion below the JT ordering temperature, as explained in Sec. V A. The extra JT energy gain for the buckled lattice is responsible for the increase in $T_{\rm JT}$ in $RE{\rm MnO_3}$ with small RE ions, as explained in Sec. V B.

wave vector $\vec{k} = (\pi,\pi)$. If this extra JT distortion is in the same [opposite] phase as [to] the deviatoric e_{3s} distortion, in other words, if $e_{20}e'_{3s}$ and e_{3s} have the same [opposite] sign, this extra JT distortion increases [decreases] the net JT distortion, which explains the expression for $E_{\rm JT}$ in Eq. (10) or $e_{\rm JT}$ in Eq. (14). We emphasize here that the extra JT energy gain occurs only when the e_2, e_3, and e'_3 distortions are in the right phase with respect to each other. Experiments[29] show that the (π,π) Mn-O-Mn bond buckling persists even above $T_{\rm JT}$ without much change in size. However, above $T_{\rm JT}$, the coherent e_3 distortion does not exist, and therefore the extra JT distortion due to the uniform e_{20} distortion in the presence of staggered buckling distortion would increase the JT energy gain in some regions and decrease the JT energy gain in other regions, and does not change the net JT energy. In other words, the energy gain due to the cooperative effect between e_3, e'_3, and e_2 does not exist at $T > T_{\rm JT}$. We therefore expect that the e_{20} mode does not exist above $T_{\rm JT}$ and appears simultaneously with the long range JT ordering, consistent with the experimental results.

B. Jahn-Teller ordering temperature and its variation among $LaMnO_3$, $PrMnO_3$, and $NdMnO_3$

It is reported[36,37] that $T_{\rm JT}$ changes from 750 K for $LaMnO_3$ to 1050 K for $PrMnO_3$, and further to 1100 K for $NdMnO_3$, that is, by about $\Delta T_{\rm JT}({\rm Pr}) = 300$ K and $\Delta T_{\rm JT}({\rm Nd}) = 350$ K relative to $LaMnO_3$ respectively, where $\Delta T_{\rm JT}(RE) = T_{\rm JT}(RE{\rm MnO_3}) - T_{\rm JT}({\rm LaMnO_3})$. We estimate $\Delta T_{\rm JT}(RE)$ from our model to understand how such a drastic change of the JT ordering temperature can occur by the increase in chemical pressure.

We rewrite $E^{\rm min}_{\rm tot}$ in Eq. (27) for $\tilde{p} > \tilde{p}_c$ as follows.

$$E^{\rm min}_{\rm tot} = -\frac{\tilde{p}^2}{2(a_1+a_2)} - \frac{\lambda^2}{2a_1} - \frac{a_1(\tilde{p}-\tilde{p}_c)^2}{2(a_1+a_2)^2}, \tag{29}$$

where

$$\tilde{p}_c = \tilde{p}^*_c - \delta\tilde{p}_c, \tag{30}$$

$$\delta\tilde{p}_c = \frac{\lambda^2}{4b_1a_1}(a_1+a_2), \tag{31}$$

and $\tilde{p}^*_c$ represents the critical chemical pressure without the JT energy term. Since $\delta\tilde{p}_c$, the change in the critical chemical pressure due to the $E_{\rm JT}$ term, is small relative to $\tilde{p} - \tilde{p}^*_c$, with $\delta\tilde{p}_c/(\tilde{p}-\tilde{p}^*_c) \approx 0.3$ for parameter values in Sec. III, we keep the terms linear in $\delta\tilde{p}_c$ only and rewrite according to the origin of each term as follows.

$$E^{\rm min}_{\rm tot} \approx E^{\rm min}_{\rm comp} + E^{\rm min}_{\rm JT} + E^{\rm min}_{\rm bk} + E^{\rm min}_{\rm bk,JT,sh}, \tag{32}$$

$$E^{\rm min}_{\rm comp} = -\frac{1}{2}\frac{\tilde{p}^2}{a_1+a_2}, \tag{33}$$

$$E^{\rm min}_{\rm JT} = -\frac{1}{2}\frac{\lambda^2}{a_1}, \tag{34}$$

$$E^{\rm min}_{\rm bk} = -\frac{1}{2}\frac{a_1}{(a_1+a_2)^2}(\tilde{p}-\tilde{p}^*_c)^2, \tag{35}$$

$$E^{\rm min}_{\rm bk,JT,sh} = -\frac{a_1}{(a_1+a_2)^2}(\tilde{p}-\tilde{p}^*_c)\delta\tilde{p}_c, \\ = -\frac{\lambda^2}{4b_1(a_1+a_2)}(\tilde{p}-\tilde{p}^*_c). \tag{36}$$

The first three terms, $E^{\rm min}_{\rm comp}$, $E^{\rm min}_{\rm JT}$, and $E^{\rm min}_{\rm bk}$, represent the energy terms purely due to compression, JT distortion, and buckling, respectively. The fourth term is the energy due to the coherent buckling, JT and shear distortions, indicated by its dependence on $\tilde{p} - \tilde{p}^*_c$, λ and b_1, which gives extra stability to the JT ordering due to the chemical pressure.

To estimate $T_{\rm JT}$, we consider a high temperature state with random JT distortions, for which the energy can be written in a similar way as Eq. (32) except for the absence of the fourth term due to the lack of coherence among distortions as explained in Sec. V A,

$$E^{\rm ran}_{\rm tot} = E^{\rm ran}_{\rm comp} + E^{\rm ran}_{\rm JT} + E^{\rm ran}_{\rm bk}. \tag{37}$$

We expect $E^{\rm ran}_{\rm comp} \approx E^{\rm min}_{\rm comp}$ and $E^{\rm ran}_{\rm bk} \approx E^{\rm min}_{\rm bk}$ since the unit cell volume and buckling angle do not change very much as the temperature crosses $T_{\rm JT}$ (Ref. 29). Therefore, the energy difference between JT ordered and JT disordered state is

$$E^{\rm ran}_{\rm tot} - E^{\rm min}_{\rm tot} \approx E^{\rm ran}_{\rm JT} - E^{\rm min}_{\rm JT} - E^{\rm min}_{\rm bk,JT,sh}. \tag{38}$$

We first verify that our model gives the correct order of magnitude of $T_{\rm JT}$ itself. An order of magnitude estimate for $T_{\rm JT}$ can be made from the energy difference between two different JT ordered states, one the most favored state and the other relatively unfavored state. The most favored state is that with the JT distortion of $\vec{k} = (\pi,\pi)$ considered so far in this paper and has the JT energy of $E^{\rm min}_{\rm JT} = -\lambda^2/(2a_1)$. We choose a state with the same size of JT distortion e_3 but with a wave vector $\vec{k} = (0,0)$ as a relatively unfavored state, with energy $E^{\rm unif}_{\rm JT} = -\lambda^2/[2(a_1+a_2)]$. Using the estimated parameter values, $a_1 = 150$ eV, $a_2 = 30$–80 eV, $\lambda = 10.8$ eV, we obtain $E^{\rm unif}_{\rm JT} - E^{\rm min}_{\rm JT} \approx 600$–$1300$ K, which has the same order of magnitude as the experimentally observed $T_{\rm JT}$ in the range of 750–1100 K.

For the change in $T_{\rm JT}$ between $LaMnO_3$ and $RE{\rm MnO_3}$ (RE = Pr, Nd), the only term in Eq. (38) which changes with the RE ion size is $-E^{\rm min}_{\rm bk,JT,shear}$. Therefore, the JT ordering temperature variation between $LaMnO_3$ and $RE{\rm MnO_3}$ can be related to $-E^{\rm min}_{\rm bk,JT,sh}(RE{\rm MnO_3}) + E^{\rm min}_{\rm bk,JT,sh}({\rm LaMnO_3})$ within a factor of the order of one. We express $E^{\rm min}_{\rm bk,JT,sh}$ in terms of $(e'_{3s})^{\rm min}$,

$$E^{\rm min}_{\rm bk,JT,sh} = -\frac{1}{2}\frac{\lambda^2}{4b_1}[(e'_{3s})^{\rm min}]^2. \tag{39}$$

According to the experimental data,[29,30,36,37] the Mn-O-Mn bond angle is 155.1° for $LaMnO_3$, 150.5° for $PrMnO_3$, and 149.8° for $NdMnO_3$, which corresponds to $(e'_{3s})^{\rm min}$ of 0.217, 0.257, and 0.264, respectively. These distortions, along with parameter values $\lambda = 10.8$ eV and $b_1 = 20$–25 eV, result in $-E^{\rm min}_{\rm bk,JT,sh}(RE{\rm MnO_3}) + E^{\rm min}_{\rm bk,JT,sh}({\rm LaMnO_3})$ of 11–14 meV $\approx$ 130–160 K for RE = Pr and 12–16 meV $\approx$ 140–190 K for RE = Nd. From a classical Monte Carlo simulation for the double-well potential model in Ref. 24, we find that the structural ordering temperature is about twice the energy difference between the distorted ground state and

undistorted high energy state.[38] Although such a relation would depend on the details of the model, if we assume a similar situation in the current model, the JT ordering temperature variation can be estimated as twice the energy difference, therefore, $T_{JT}(NdMnO_3) - T_{JT}(LaMnO_3) \approx 2 \times [-E^{min}_{bk,JT,sh}(NdMnO_3) + E^{min}_{bk,JT,sh}(LaMnO_3)] = 300$–$375$ K, which agrees well with the experimental change in T_{JT}, 350 K. Similar analysis for $PrMnO_3$ leads to $T_{JT}(PrMnO_3) - T_{JT}(LaMnO_3) \approx 255$–$320$ K, which agrees well with the experimental value of 300 K.

This agreement shows that indeed the JT ordered state is more stabilized when the buckling increases for smaller RE ions for undoped compounds. The relatively large increase in the JT ordering temperature, both in theory and experimental data, shows that the interplay between the RE ion size and the JT distortion is significant, and should be taken into account to explain the well-known temperature-tolerance factor phase diagram of both undoped and doped perovskite manganites.

C. Relation between shear, buckling, and deviatoric distortion and comparison for other undoped manganites

Equations (22) and (25) imply that the following quantities remain constant regardless of the variation in chemical pressure:

$$(e_{3s})^{min} = \frac{\lambda}{a_1}, \tag{40}$$

$$\frac{(e_{20})^{min}}{(e'_{3s})^{min}} = \frac{\lambda}{4b_1}, \tag{41}$$

$$\frac{(e_{20})^{min}}{(e_{3s})^{min}(e'_{3s})^{min}} = \frac{a_1}{4b_1}. \tag{42}$$

We calculate these quantities from the experimental data for $LaMnO_3$, $PrMnO_3$, and $NdMnO_3$, and present the results in Table I, in which we also show the relation between the distortion variables in our model and experimental parameters and the estimate of T_{JT} and ΔT_{JT} obtained in Sec. V B. The results show that $(e_{3s})^{min}$, $(e_{20})^{min}/(e'_{3s})^{min}$, and $(e_{20})^{min}/[(e_{3s})^{min}(e'_{3s})^{min}]$ agree well with theoretical estimates obtained from the parameters in Sec. III, and vary 7%, 29%, and 32%, respectively, smaller than up to 41% changes in $(e_{20})^{min}$ and $(e'_{3s})^{min}$. The results underscore the strong coupling between these distortions, in particular, the important role played by the uniform shear distortion in connecting the JT and buckling distortions.

We extend the analysis to undoped perovskite manganites with even smaller RE ions. The results are summarized in Fig. 7, along with values from available experimental data. Figure 7(a) shows the JT ordering temperature variation with respect to $LaMnO_3$ from our theory along with measured T_{JT} for $LaMnO_3$, $PrMnO_3$, and $NdMnO_3$, which indicates rapid increase of the JT energy gain as the RE size becomes smaller. Figure 7(b) shows that the ratio e_{20}/e'_{3s} from experimental data remains relatively close to the range of theoretical constant ratios of $\lambda/(4b_1)$. Explanation for the deviation from theoretically estimated constant for the whole range of RE ions may require higher order expansions of the energy expression. Figure 7(c) shows e_{JT} from experimental data and theory. For the experimental data, e_{JT} is calculated from $(l - s)/u$, where l and s are in-plane long and short Mn-O bond lengths, as in Table I. Theoretical range of e_{JT} versus e'_{3s} is from $e_{JT} \approx e_{3s} + e_{20}e'_{3s}$ with $e_{3s} \approx \lambda/a_1$ and $e_{20} \approx e'_{3s}\lambda/(4b_1)$. Both theory and experiment consistently show an overall increase of e_{JT} as Mn-O-Mn bond buckling increases.

VI. DISCUSSION ON HOW TO EXTEND THE MODEL TO DOPED MANGANITES AND ELECTRONICALLY FERROELECTRIC UNDOPED MANGANITES

Although the primary focus of this paper is the high temperature JT structural phase transition in undoped perovskite

TABLE I. Parameters from experimental data and comparison with theoretical estimates. Experimental data for the lattice constants, bond lengths, and bond angles for $LaMnO_3$, $PrMnO_3$ and $NdMnO_3$ are from Refs. 29, 30, 36, and 39, measured at room temperature.

	Experimental data			
Parameters	$LaMnO_3$	$PrMnO_3$	$NdMnO_3$	Theoretical estimates
Lattice constant, a	5.54 Å	5.45 Å	5.41 Å	
Lattice constant, b	5.75 Å	5.81 Å	5.73 Å	
Long Mn-O bond length within ab plane, l	2.18 Å	2.21 Å	2.20 Å	
Short Mn-O bond length within ab plane, s	1.91 Å	1.91 Å	1.90 Å	
Mn-O-Mn bond angle within ab plane, φ	155.1°	150.5°	149.8°	
Mn-Mn distance with e_{10} only, $(a + b)/(2\sqrt{2})$	3.99 Å	3.98 Å	3.94 Å	Compressed from $u \approx 4$ Å
$e_{20} = (b - a)/(2\sqrt{2}u)$	0.0186	0.0322	0.0280	
$e'_{3s} = (\pi - \varphi)/2$	0.217	0.257	0.264	
e_{20}/e'_{3s}	0.086	0.125	0.106	$\lambda/(4b_1) = 0.108$–0.135
$e_{JT} = (l - s)/u$	0.0678	0.0753	0.0750	
$e_{3s} \approx e_{JT} - e_{20}e'_{3s}$	0.0637	0.0670	0.0676	$\lambda/a_1 = 0.072$
$e_{20}/(e_{3s}e'_{3s})$	1.35	1.86	1.57	$a_1/(4b_1) = 1.5$–1.9
T_{JT}	750 K	1050 K	1100 K	$E^{unif}_{JT} - E^{min}_{JT} = 600$–$1300$ K
$\Delta T_{JT}(Pr) = T_{JT}(PrMnO_3) - T_{JT}(LaMnO_3)$		300 K		$-2\Delta E^{min}_{bk,JT,sh} = 255$–$320$ K
$\Delta T_{JT}(Nd) = T_{JT}(NdMnO_3) - T_{JT}(LaMnO_3)$			350 K	$-2\Delta E^{min}_{bk,JT,sh} = 300$–$375$ K

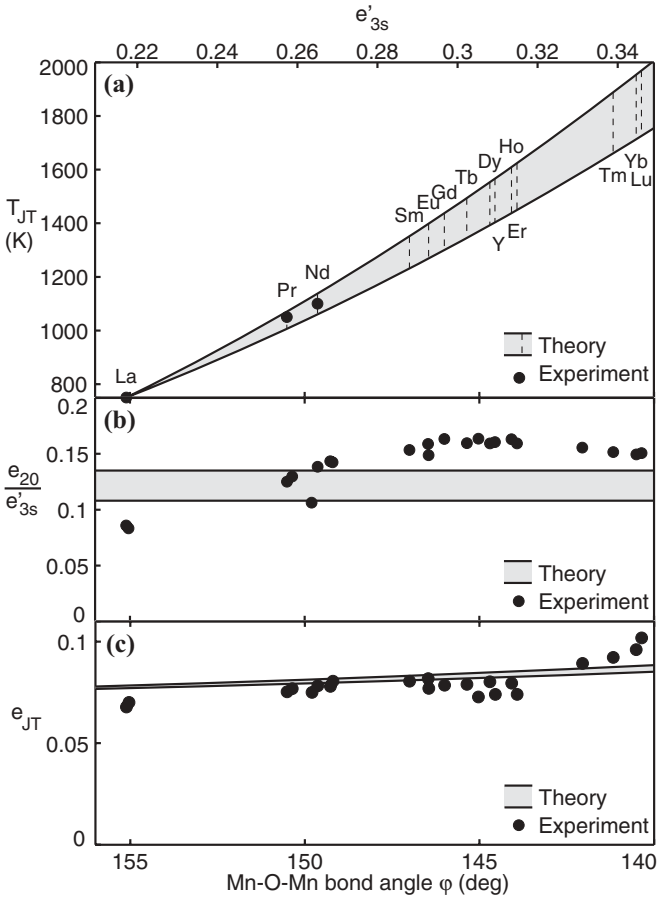

FIG. 7. Available experimental data and bounds estimated from theory, plotted against Mn-O-Mn bond angle and e'_{3s}, for (a) JT ordering temperature, (b) e_{20}/e'_{3s} ratio, and (c) e_{JT}. Experimental data are from Refs. 36,39–41, and references therein.

manganites, we briefly comment in this section on how to extend the model to doped manganites and electronically ferroelectric undoped manganites. In the case of doped manganites, each Mn site has a fractional number of $3d$ e_g electrons, which would require quantum mechanical description of e_g electrons, similar to the ones in Refs. 7–11. Furthermore, RE and AK ions with different sizes distribute randomly, effectively generating site-dependent chemical pressure. Experimentally, it is observed that the increased variance of RE and AK ion sizes has a similar effect as the decreased average RE and AK ion size in doped manganites. If we focus on the effects of chemical pressure, the first necessary modification to the existing models in Refs. 7–11 would be a classical coupling between local chemical pressure and local dilatation mode of surrounding O ions, similar to e'_1. The second necessary modification would be anharmonic lattice energy terms obtained from the Keating model, similar to the ones presented in this paper. Because chemical pressure $\tilde{p}_{\vec{i}}$ is dependent on site, we should consider all modes shown in Fig. 3 at each site and the constraints between Fourier transforms of these variables, instead of just the four modes in Fig. 4. With many variables involved, numerical approaches, such as Monte Carlo methods, would be essential.

Our model can be extended and serve as a phenomenological model for the magnetism and electronic ferroelectricity in undoped manganites,[12,37,41] complementing existing theories, such as the ones based on local density approximation.[13] In undoped manganites, the magnetic interaction also shows a prominent dependence on the size of RE ions, changing the ground state from A-type to E-type antiferromagnetic phase through incommensurate phases as RE ion becomes smaller. This behavior has been proposed to originate from the reduced nearest neighbor ferromagnetism and the increased next nearest neighbor antiferromagnetism,[37] or alternatively, the reduced antiferromagnetism between t_{2g} spins and long range ferromagnetic double exchange interaction.[11] It has been further proposed that electronically ferroelectric phase may emerge in E-type antiferromagnetic phase, associated with the displacement of Wannier function center (WFC) from the ionic location due to the magnetic inversion symmetry breaking for E-type spin ordering.[13] Within our phenomenological approach, the dependence of the first nearest and the second nearest neighbor magnetic interaction J_1 and J_2 on the Mn-O-Mn bond buckling can be expressed as $J_1 = J_{10}(1 + \alpha_1 e'_{3s})$ and $J_2 = J_{20}(1 + \alpha_2 e'_{3s})$ for a small range of e'_{3s}, in which the linear coefficients α_1 and α_2 can be decided from more fundamental theories. The t_{2g}-t_{2g} super-exchange interaction can be expressed in a similar way.

As for the electronic ferroelectricity, although the explicit form of the Wannier function would require quantum mechanical analysis, the WFC itself can be treated as a classical variable and the lattice of the WFC can be considered in addition to the lattice of Mn ions. Therefore, symmetry-based analysis can be applied to both the WFC lattice and the ionic lattice. To demonstrate the idea, we consider an example of three connected Mn-O motifs at sites (−1,0), (0,0), and (1,0) shown in Fig. 8. The x directional displacement of Mn ion at site $\vec{i}$, the x directional displacement of WFC associated with Mn $3d_{3x^2-r^2}$ state with spin parallel to the t_{2g} core spin at site $\vec{i}$, and the t_{2g} spin at site $\vec{i}$ with magnitude of $|S_{t_{2g}}|$ are represented by $d_{\vec{i}}$, $D_{\vec{i}}$, and $\vec{S}_{\vec{i}}$. We also consider the buckling distortion e'_{3s}. If we consider a situation without any other distortions, the energy associated with these limited degrees

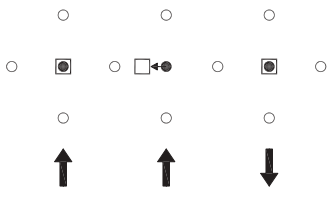

FIG. 8. Schematic drawing that demonstrates how our model can be extended to include electronic ferroelectricity in undoped manganites. Three connected MnO_4 motifs are shown. Open and solid circles represent O and Mn ions. Open squares represent WFC's associated with the Mn $3d_{3x^2-r^2}$ state with spin parallel to the t_{2g} core spin, which would coincide with Mn ions in the nonferroelectric phase. Thick arrows at the bottom represent the t_{2g} spin directions for E-type antiferromagnetic phase of undoped manganites. Thin horizontal arrow represents the displacement of WFC from Mn ion location, resulting in the ferroelectric moment of electronic origin.

of freedom can be written in the following form based on the symmetry:

$$E_{\mathrm{eFE}} = \frac{K_d}{2}\left(d_{(-1,0)}^2 + d_{(0,0)}^2 + d_{(1,0)}^2\right) + \frac{K_D}{2}[(D_{(-1,0)} - d_{(-1,0)})^2 + (D_{(0,0)} - d_{(0,0)})^2 + (D_{(1,0)} - d_{(1,0)})^2] + J_{10}\vec{S}_{(-1,0)} \cdot \vec{S}_{(0,0)}[1 + \alpha_1 e'_{3s} + \beta(D_{(0,0)} - D_{(-1,0)})] + J_{10}\vec{S}_{(0,0)} \cdot \vec{S}_{(1,0)}[1 + \alpha_1 e'_{3s} + \beta(D_{(1,0)} - D_{(0,0)})], \quad (43)$$

where the terms with β represent how the magnetic interaction depends on the distance between the nearest neighbor WFC's. In the case of $d_{(0,0)} = d_{(-1,0)} = d_{(1,0)} = 0$ due to other elastic energy terms that are not considered above and $\vec{S}_{(-1,0)} = \vec{S}_{(0,0)} = -\vec{S}_{(1,0)}$ due to the E-type magnetic ordering, the minimization with respect to $D_{(0,0)}$ leads to $D_{(0,0)} = -2J_{10}|S_{t_{2g}}|^2\beta/K_D$, shown schematically in Fig. 8 with a thin arrow and an open square representing WFC, which demonstrates how our model can be expanded to model ferroelectric moment of electronic origin. Our symmetry-mode-based approach can be also used to model conventional ionic ferroelectricity in perovskite transition metal oxides by including energy terms with inversion symmetry breaking modes, such as t_x, t_y, t'_x, and t'_y in Fig. 3.

VII. CONCLUSION

From the analysis of a Keating energy expression expanded in terms of the atomic-scale symmetry-modes, we find that the effect of small RE ion size, known as chemical pressure effect, is significant in stabilizing the long range JT distortion in undoped perovskite manganites. We obtain good agreement with the experimental data on the JT ordering temperature and the substantial increase of the JT ordering temperature from $LaMnO_3$ to $PrMnO_3$ and $NdMnO_3$. We propose that similar effects need to be considered to understand the phase diagram for doped perovskite manganites. We also explain the appearance of the uniform shear distortion below the JT ordering temperature in terms of the coupling between coherent shear, buckling, and deviatoric distortions within the JT energy. Moreover, we estimate the ratio between these distortions at low temperature, and find good agreement with experimental data for $LaMnO_3$, $PrMnO_3$, and $NdMnO_3$, which confirms the coupling proposed between them in our model.

ACKNOWLEDGMENTS

This work was supported by US DOE/LANL Award No. DE-AC52-06NA25396/170590-1 (T.F.S., K.H.A.), ANL XSD Visitor Program (K.H.A.), NJIT (T.F.S., K.H.A.), US DOE LANL LDRD (T.L., A.S., A.R.B.), and DOE FWP 70069 (P.B.L.).

*Correspondence should be addressed to: kenahn@njit.edu

[1] R. von Helmolt, J. Wecker, B. Holzapfel, L. Schultz, and K. Samwer, Phys. Rev. Lett. **71**, 2331 (1993).
[2] S. Jin, T. H. Tiefel, M. McCormack, R. A. Fastnacht, R. Ramesh, and L. H. Chen, Science **264**, 413 (1994).
[3] M. B. Salamon and M. Jaime, Rev. Mod. Phys. **73**, 583 (2001).
[4] A. J. Millis, P. B. Littlewood, and B. I. Shraiman, Phys. Rev. Lett. **74**, 5144 (1995).
[5] A. J. Millis, B. I. Shraiman, and R. Mueller, Phys. Rev. Lett. **77**, 175 (1996).
[6] H. Röder, J. Zang, and A. R. Bishop, Phys. Rev. Lett. **76**, 1356 (1996).
[7] J. A. Vergés, V. Martín-Mayor, and L. Brey, Phys. Rev. Lett. **88**, 136401 (2002).
[8] A. Moreo, S. Yunoki, and E. Dagotto, Science **283**, 2034 (1999).
[9] S. Kumar and P. Majumdar, Phys. Rev. Lett. **96**, 016602 (2006).
[10] K. Pradhan, A. Mukherjee, and P. Majumdar, Phys. Rev. Lett. **99**, 147206 (2007).
[11] J. Salafranca and L. Brey, Phys. Rev. B **73**, 024422 (2006).
[12] I. A. Sergienko, C. Şen, and E. Dagotto, Phys. Rev. Lett. **97**, 227204 (2006).
[13] K. Yamauchi, F. Freimuth, S. Blügel, and S. Picozzi, Phys. Rev. B **78**, 014403 (2008).
[14] H. Y. Hwang, S.-W. Cheong, P. G. Radaelli, M. Marezio, and B. Batlogg, Phys. Rev. Lett. **75**, 914 (1995).
[15] M. O. Dzero, L. P. Gorkov, and V. Z. Kresin, Eur. Phys. J. B **14**, 459 (2000).
[16] J. A. Fernandez-Baca, P. Dai, H. Y. Hwang, C. Kloc, and S.-W. Cheong, Phys. Rev. Lett. **80**, 4012 (1998).
[17] J. W. Liu, Z. Zeng, Q. Q. Zheng, and H. Q. Lin, Phys. Rev. B **60**, 12968 (1999).
[18] J. W. Lynn, R. W. Erwin, J. A. Borchers, Q. Huang, A. Santoro, J.-L. Peng, and Z. Y. Li, Phys. Rev. Lett. **76**, 4046 (1996).
[19] P. G. Radaelli, G. Iannone, M. Marezio, H. Y. Hwang, S.-W. Cheong, J. D. Jorgensen, and D. N. Argyriou, Phys. Rev. B **56**, 8265 (1997).
[20] D. Louca, T. Egami, W. Dmowski, and J. F. Mitchell, Phys. Rev. B **64**, 180403(R) (2001).
[21] A. J. Millis, Phys. Rev. B **53**, 8434 (1996).
[22] T. Kimura, T. Goto, H. Shintani, K. Ishizaka, T. Arima, and Y. Tokura, Nature (London) **426**, 55 (2003).
[23] K. H. Ahn and A. J. Millis, Phys. Rev. B **64**, 115103 (2001).
[24] K. H. Ahn, T. Lookman, A. Saxena, and A. R. Bishop, Phys. Rev. B **68**, 092101 (2003).
[25] K. H. Ahn, T. Lookman, and A. R. Bishop, Nature (London) **428**, 401 (2004).
[26] The normalization factor is chosen in such a way that, for example, $e_3 = 2d_O$ if each O ion around Mn ion is displaced by d_O in the way shown in Fig. 3.
[27] P. N. Keating, Phys. Rev. **145**, 637 (1966).
[28] P. B. Littlewood, Phys. Rev. B **34**, 1363 (1986).
[29] J. Rodríguez-Carvajal, M. Hennion, F. Moussa, A. H. Moudden, L. Pinsard, and A. Revcolevschi, Phys. Rev. B **57**, R3189 (1998).
[30] A. M. Balagurov, S. N. Bushmeleva, V. Yu. Pomjakushin, D. V. Sheptyakov, V. A. Amelichev, O. Yu. Gorbenko, A. R. Kaul, E. A. Gan'shina, and N. B. Perkins, Phys. Rev. B **70**, 014427 (2004).
[31] T. W. Darling, A. Migliori, E. G. Moshopoulou, S. A. Trugman, J. J. Neumeier, J. L. Sarrao, A. R. Bishop, and J. D. Thompson, Phys. Rev. B **57**, 5093 (1998).
[32] N. W. Ashcroft and N. D. Mermin, *Solid State Physics* (Holt, Rinehart and Winston, New York, 1976), pp. 443–447.

[33] A. P. Mirgorodsky and M. B. Smirnov, J. Phys.: Condens. Matter. **5**, 3313 (1993).
[34] J. Zhang, P. Dai, J. A. Fernandez-Baca, E. W. Plummer, Y. Tomioka, and Y. Tokura, Phys. Rev. Lett. **86**, 3823 (2001).
[35] K. H. Ahn and A. J. Millis, Phys. Rev. B **61**, 13545 (2000).
[36] D. Sanchez, J. A. Alonso, and M. J. Martinez-Lope, J. Chem. Soc. Dalton Trans. **23**, 4422 (2002).
[37] T. Kimura, S. Ishihara, H. Shintani, T. Arima, K. T. Takahashi, K. Ishizaka, and Y. Tokura, Phys. Rev. B **68**, 060403(R) (2003).
[38] We carry out classical Monte Carlo simulations with the same energy expression and parameter values used for the results in Fig. 3 of Ref. 24. We find that the structural phase transition temperature is about 0.15, which is about twice the depth of the potential well 0.08.
[39] K. Liu, X. W. Wu, K. H. Ahn, T. Sulchek, C. L. Chien, and J. Q. Xiao, Phys. Rev. B **54**, 3007 (1996).
[40] J. A. Alonso, M. J. Martínez-Lope, M. T. Casais, and M. T. Fernández-Díaz, Inorg. Chem. **39**, 917 (2000).
[41] M. Mochizuki and N. Furukawa, Phys. Rev. B **80**, 134416 (2009).